Heart and Vessels (2020) 35:38–45
https://doi.org/10.1007/s00380-019-01461-7

ORIGINAL ARTICLE

Optical coherence tomography characteristics of in-stent restenosis after drug-eluting stent implantation: a novel classification and its clinical significance

Wataru Yamamoto[1] · Kenichi Fujii[1] · Satoru Otsuji[1] · Shin Takiuchi[1] · Mikio Kakishita[1] · Motoaki Ibuki[1] · Katsuyuki Hasegawa[1] · Kasumi Ishibuchi[1] · Hiroto Tamaru[1] · Shingo Yasuda[1] · Rui Ishii[1] · Sho Nakabayashi[1] · Hirofumi Kusumoto[1] · Yorihiko Higashino[1]

Received: 17 December 2018 / Accepted: 21 June 2019 / Published online: 27 June 2019

Abstract

This study aimed to establish a novel classification of in-stent restenosis (ISR) morphological characteristics after drug-eluting stent (DES) implantation as visualized by optical coherence tomography (OCT) and determine its clinical significance. A total of 133 lesions with intrastent restenosis after DES implantation were imaged by OCT. Neointimal tissue characteristics were categorized according to the classical classification as either homogeneous, heterogeneous, or layered. Then all tissues were also classified into six types as follows: homogeneous high-intensity tissue (type I), heterogeneous tissue with signal attenuation (type II), speckled heterogeneous tissue (type III), heterogeneous tissue containing poorly delineated region with invisible strut (type IV), heterogeneous tissue containing sharply delineated low-intensity region (type V), or bright protruding tissue with an irregular surface (type VI). The kappa value for interobserver agreement between the two observers was higher in the modified classification than in the classical classification (0.97 and 0.72, respectively). Most lesions classified as type V and VI were likely to be identified in patients on hemodialysis and located at the ostial right coronary artery. The duration from stent implantation to ISR was significantly longer in types IV and VI than in others. The incidence of stent fracture was significantly higher in types I and IV. This new modified classification enabled us to classify most ISR lesions easily with higher reproducibility. The clinical significance of neointimal restenotic tissue classification by OCT became clear while using the modified classification.

Keywords Classifications · Optical coherence tomography · In-stent restenosis · Drug-eluting stent

Abbreviations

CAG	Coronary angiography
DES	Drug-eluting stent
ISR	In-stent restenosis
MLA	Minimal lumen area
NIH	Neointimal hyperplasia
OCT	Optical coherence tomography

Introduction

Intracoronary optical coherence tomography (OCT), a catheter-based imaging modality for the visualization of coronary arteries, is widely used during percutaneous coronary intervention. This technology allows for an increased understanding of the anatomy of lesions and helps elucidate the mechanisms of atherosclerosis. As cross-sectional images of OCT are generated by measuring the echo time delay and intensity of light that is reflected or backscattered from the tissue, OCT has the potential to characterize tissue morphology in vivo. In 2009, Gonzalo et al. [1] reported that the appearance of in-stent restenosis (ISR) tissue on OCT could be classified as either homogeneous, heterogeneous, or layered type. Over the years, this classification has been widely adopted in both clinical practice and research for differentiating tissue components after stent implantation [2–4]. However, in daily clinical practice, it is common

✉ Kenichi Fujii
fujiik@hirakata.kmu.ac.jp

[1] Department of Cardiology, Higashi Takarazuka Satoh Hospital, Takarazuka 6650873, Hyogo, Japan

to encounter ISR tissue that cannot be classified using this classification [5–7]. Moreover, there is no appropriate classification for "in-stent neoatherosclerosis", which is defined as atherosclerotic changes in the neointimal tissue. These changes constitute a possible risk factor for late stent thrombosis [8, 9]. Therefore, this study aimed to establish a new classification of ISR morphological characteristics after drug-eluting stent (DES) implantation as visualized by OCT and determine its clinical significance.

Methods

Patient populations

This was a retrospective observational study at a single center (Higashi Takarazuka Satoh Hospital, Takarazuka, Japan). All patients treated by a repeat intervention using OCT due to symptomatic or hemodynamically significant intrastent restenosis after DES implantation between January 2011 and December 2017 were selected from our prospectively maintained database and analyzed retrospectively. The exclusion criteria were (1) stent thrombosis in the 4 weeks prior to the OCT procedure, (2) minimum lumen area (MLA) located outside of the stent contour, (3) recurrent ISR lesions, (4) in-stent total occlusion lesions, (5) balloon pre-dilatation before OCT examination, and (6) poor OCT image quality. After DES implantation, dual antiplatelet therapy was recommended for at least 12 months in all patients, and consisted of a combination of aspirin (100 mg/day) and clopidogrel (75 mg/day) or prasugrel (5 mg/day). Aspirin (100 mg/day) was continued indefinitely thereafter. Angiographic follow-up was not mandatory unless there were clinical symptoms or subjective evidence of ischemia on functional testing. All patients provided written informed consent, and the institutional review boards at our center approved this study.

Quantitative coronary angiographic analysis

Coronary angiography (CAG) was performed after intracoronary administration of 0.2 mg nitroglycerin. Quantitative CAG was performed as the first procedure, in the respective ISR phase, using a guiding catheter to calibrate the magnification and a validated automated edge detection algorithm (CAAS 5.11, Pie Medical Imaging, Eindhoven, The Netherlands). The minimum lumen diameter, reference diameter, and lesion length were measured.

OCT image acquisition

OCT image acquisition was performed after diagnostic CAG and before percutaneous coronary intervention, using either a time- or frequency-domain OCT system. A time-domain OCT (TD-OCT, M2 OCT system, LightLab Imaging Inc., Westford, MA, USA) was performed by the occlusive technique. An over-the-wire occlusion balloon catheter (Helios, LightLab Imaging Inc., Westford, MA, USA) was advanced over a 0.016-in. imaging wire (ImagingWire, LightLab Imaging Inc., Westford, MA, USA) and held in place across the stented segment. The occlusion balloon was then inflated to 0.6 atm, while 0.9% saline was infused from the distal tip of the occlusion balloon at 0.5 mL/s to clear the imaging field. An imaging run was performed from the distal to proximal site of the stented segment using automated transducer pullback at 1.0 mm/s [10]. All images were acquired at 15.6 frames/s. In contrast, the frequency-domain OCT was performed using a non-occlusive technique. A frequency-domain OCT catheter (FastView, Terumo, Tokyo, Japan, or C7 Dragonfly, Abbott Vascular, Santa Clara, CA, USA) was advanced to the distal portion of the stented segment through an angioplasty guidewire. To remove blood cells from the view area, contrast medium was continuously flushed from the guiding catheter, while the OCT was being performed, using automatic pullback devices at 20 mm/s. OCT images were digitally stored for offline analysis.

OCT image analysis

Quantitative OCT assessments were performed at the minimal lumen area (MLA) site and at the proximal and distal reference sites. The lumen and stent were manually traced, and the area of neointimal hyperplasia (NIH = stent area minus lumen area) was calculated for each frame. The percent NIH area was also calculated as follows: (NIH area/stent area) × 100. Percent stent expansion was measured as follows: the stent area at the MLA site divided by the average of the proximal and distal reference lumen area. An ISR was defined as edge if the MLA site was located within 5 mm from the end of the DES, but in the stented segments. The qualitative morphological appearance of the neointima was assessed at the MLA and at two 1-mm intervals proximal and distal to the MLA, and the predominant one was chosen for the analysis. First, neointimal tissue characteristics were categorized as follows: (1) a homogeneous neointima, defined as one that had a uniform signal-rich band without focal variation or attenuation; (2) a heterogeneous neointima, defined as one with focally changing optical properties and various backscattering patterns; and (3) a layered neointima, defined as one with layers having different optical properties (i.e., an abluminal high-scattering layer and abluminal low-scattering layer) [1, 11]. A stent fracture was defined as the absence of stent struts over one-half or more of the stent circumference on OCT image [12]. All OCT images were reviewed by two experienced independent observers who

were blinded to patient information. After reviewing all OCT images, a single observer also classified neointimal tissue characteristics into six patterns as follows (Fig. 1):

Type I: "Homogeneous high-intensity tissue" ISR. The homogeneous high-intensity tissue is characterized by a uniform signal-rich band without signal attenuation. Stent struts behind these tissues were visible.

Type II: "Heterogeneous tissue with signal attenuation" ISR. Heterogeneous tissue with gradual signal attenuation with diffusely delineated borders and heterogeneous low signal intensity band with high-intensity band adjacent to the luminal surface with signal attenuation. Stent struts behind these tissues are visible.

Type III: "Speckled heterogeneous tissue" ISR. Speckled heterogeneous tissue appears to constitute the majority of the tissue showing low backscatter and a mottled pattern. Stent struts behind these tissues are visible.

Type IV: "Heterogeneous tissue containing poorly delineated region with invisible strut" ISR. Heterogeneous tissue comprising poorly delineated regions with invisible strut and characterized by a signal-intensity-poor region. Stent struts behind these tissues are invisible.

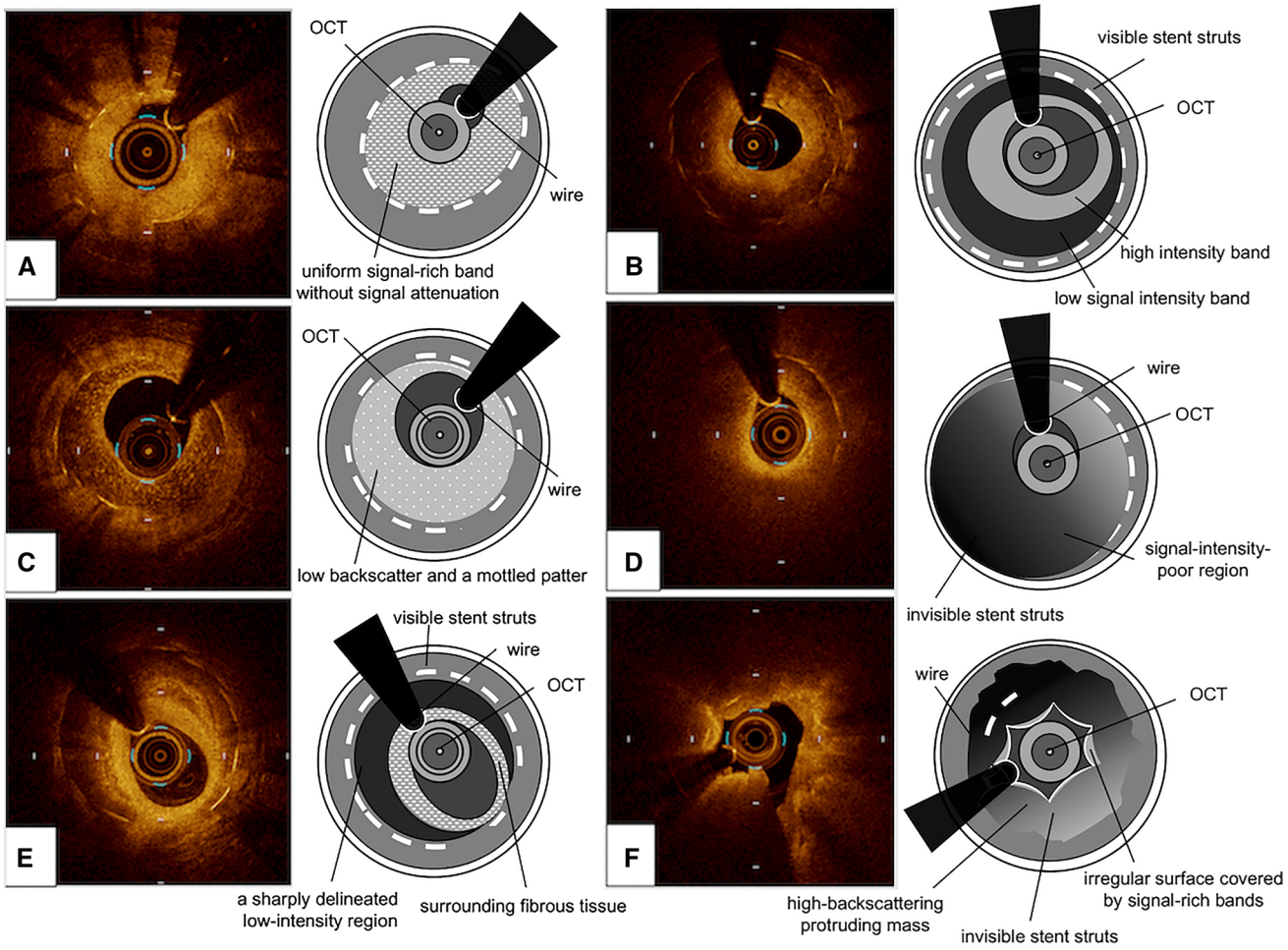

Fig. 1 Modified classification of restenotic tissue after DES implantation. **a** Type I appeared as "Homogeneous high-intensity tissue". The homogeneous high-intensity tissue is characterized by a uniform signal-rich band without signal attenuation. Stent struts behind these tissues were visible. **b** Type II appeared as "Heterogeneous tissue with signal attenuation" ISR. Heterogeneous tissue with signal attenuation and heterogeneous low signal intensity band with high-intensity band adjacent to the luminal surface with signal attenuation. Stent struts behind these tissues are visible. **c** Type III appeared as "Speckled heterogeneous tissue" ISR. Speckled heterogeneous tissue appears to constitute the majority of the tissue showing low backscatter and a mottled pattern. Stent struts behind these tissues are visible. **d** Type IV appeared as "Heterogeneous tissue containing poorly delineated region with invisible strut" ISR. Heterogeneous tissue comprising poorly delineated regions with invisible strut and characterized by a signal-intensity-poor region. Stent struts behind these tissues are invisible. **e** Type V appeared as "Heterogeneous tissue containing sharply delineated low-intensity region" ISR. The heterogeneous tissue containing a sharply delineated low-intensity region has a signal-intensity-poor region, with sharply delineated borders within the surrounding fibrous tissue. Stent struts behind these tissues were visible. **f** Type VI appeared as "Bright protruding tissue with an irregular surface" ISR. The bright protruding tissue with an irregular surface appears as a high-backscattering protruding mass with an irregular surface covered by signal-rich bands adjacent to the luminal surface. Stent struts behind these tissues are invisible. *DES* drug-eluting stent

Type V: "Heterogeneous tissue containing sharply delineated low-intensity region" ISR. The heterogeneous tissue containing a sharply delineated low-intensity region has a signal-intensity-poor region, with sharply delineated borders within the surrounding fibrous tissue. Stent struts behind these tissues were visible.

Type VI: "Bright protruding tissue with an irregular surface" ISR. The bright protruding tissue with an irregular surface appears as a high-backscattering protruding mass with an irregular surface covered by signal-rich bands adjacent to the luminal surface. Stent struts behind these tissues are invisible.

The interobserver agreements for the assessment of neointimal tissue morphology for both classical and modified classifications were evaluated.

Statistical analysis

As this is an observational, exploratory study, no formal sample size calculation was performed. Continuous variables are presented as mean ± standard deviation and analyzed using one-way analysis of variance with Tukey's test for post hoc comparisons. Categorical variables are presented as counts and percentages, and were compared using the Chi-square test or Fisher exact test. A kappa test was used to evaluate the interobserver and intraobserver variability for qualitative OCT assessment. A P value < 0.05 was considered statistically significant. All tests were performed using JMP 11 (SAS Institute).

Results

Clinical characteristics

During the study period, 590 percutaneous coronary interventions were performed in our hospital for ISR lesions. Of these, total of 133 ISR lesions were analyzed in this study. The baseline patient characteristics are shown in Table 1. The median duration of ISR presentation from initial stent implantation was 16 months. Of the ISRs, 47% (63 lesions) occurred within 1 year, 15% (20 lesions) within 1–2 years, 7% (9 lesions) within 2–3 years, 7% (9 lesions) within 3–4 years, 5% (7 lesions) within 4–5 years, and 19% (25 lesions) after 5 years. The original target lesion was chronic total occlusion in 11% (14 lesions). At the time of ISR, 11% of patients presented with acute coronary syndrome, 61% were asymptomatic, and 28% were diagnosed with stable angina pectoris.

Table 1 Baseline characteristics

Demographics	
Age (years)	71 ± 10
Male	102 (77)
Hypertension	115 (86)
Dyslipidemia	88 (66)
Diabetes mellitus	66 (50)
Current smoker	35 (26)
Family history of coronary artery disease	16 (12)
Hemodialysis	13 (10)
Previous myocardial infarction	42 (32)
History of coronary artery bypass grafting	11 (8)
Clinical presentation at the time of stent implantation	
Asymptomatic	49 (37)
Stable angina	51 (38)
Acute coronary syndrome	33 (25)
Target vessel	
Left anterior descending	65 (49)
Left circumflex	23 (17)
Right coronary	45 (34)
Type of drug-eluting stents	
First generation	47 (35)
Second generation	86 (65)

Data given as mean ± SD or *n* (%)

Angiographic analysis

The pattern of ISR was mostly focal (70%), and most ISRs (65%) were identified at the body of the stent. Forty-seven lesions (35%) were observed at the edge of the stent; 27 lesions were located at the proximal edge, and 20 lesions at the distal edge of the stents.

The classical classification of ISR tissue

Tissues were classified using the Gonzalo's classification as follows: 14 lesions (11%) were classified as homogeneous, 33 (25%) as heterogeneous, and 86 (64%) as layered. Kappa measure of agreement for interobserver agreement was 0.72 and 0.82 for intraobserver variability. Disagreement between the two observers was noted in the classification of 20 lesions. In 17 of these 20 cases (85%), a lesion classified as a heterogeneous neointima by one observer was classified as a layered neointima by the other observer.

The modified classification and its clinical features

According to the modified classification system, 14 (11%), 64 (48%), 20 (15%), 23 (17%), 6 (5%), and 6 (5%) lesions were classified as types I, II, III, IV, V, and VI, respectively. Kappa measure of agreement for interobserver agreement

was 0.97 and 0.96 for intraobserver variability. Disagreement between the two observers was noted in only two cases. Of 14 homogeneous lesions on the classical OCT classification, 13 were classified as type I and 1 was classified as type II by the modified classification. Of 33 heterogeneous lesions, 20 were categorized as type III, 10 type IV, 2 type V, and 1 type VI by the modified classification. Of 86 layered lesions on the classical OCT classification, 1 was classified as type I, 63 type II, 14 type IV, 4 type V, and 4 type VI by the modified classification. Clinical, lesion, and stent characteristics for each type of ISR are summarized in Table 2. Although there were no significant differences in cardiovascular risk factors among ISR types, most of ISR lesions classified as type V and VI were likely to be identified in patients on hemodialysis and located at the ostial right coronary artery. The duration from stent implantation to ISR was significantly longer in types IV and VI than in others. The average percentage of stent expansion was > 90% in all ISR types, with no significant difference. The incidence of stent fracture was significantly higher in types I and IV. Most stent fractures were identified in the middle RCA for type IV lesions and in the ostial RCA for type VI lesions. Microvessels within the neointima were frequently identified in type II and III lesions. Neointimal rupture was found in only two lesions (1%), both of which were classified as type IV (Table 3).

Discussion

The main findings of the present study are as follows: (1) some of the ISR tissue could not be classified into any specific type using the classical OCT classification. This could have led to the low reproducibility between the observers;

Table 2 Clinical, lesion, and stent characteristics

	Type I ($n=14$)	Type II ($n=64$)	Type III ($n=20$)	Type IV ($n=23$)	Type V ($n=6$)	Type VI ($n=6$)	P value
Hypertension	14 (100)	51 (80)	19 (95)	22 (96)	4 (67)	5 (86)	0.04
Dyslipidemia	8 (57)	43 (67)	13 (65)	15 (65)	5 (83)	4 (67)	0.92
Diabetes mellitus	7 (50)	32 (50)	9 (45)	10 (43)	5 (83)	3 (50)	0.62
Current smoker	2 (14)	20 (31)	7 (35)	3 (13)	1 (17)	2 (33)	0.39
Hemodialysis	2 (14)	4 (6)	0 (0)	1 (4)	3 (50)	3 (50)	0.002
Clinical presentation at baseline							0.77
Asymptomatic	4 (29)	26 (41)	7 (35)	8 (35)	3 (50)	1 (17)	
Stable angina	8 (57)	23 (36)	6 (30)	10 (43)	1 (17)	3 (50)	
Acute coronary syndrome	2 (14)	15 (23)	7 (35)	5 (22)	2 (33)	2 (33)	
Clinical presentation at ISR							0.20
Asymptomatic	11 (79)	34 (54)	15 (75)	13 (56)	5 (83)	2 (33)	
Stable angina	3 (21)	21 (33)	4 (20)	5 (22)	1 (17)	3 (50)	
Unstable angina	0 (0)	8 (13)	1 (5)	5 (22)	0 (0)	1 (17)	
Duration for ISR (days)	596 ± 864	748 ± 748	739 ± 843	1729 ± 1007	524 ± 439	1027 ± 849	< 0.001
Stented artery							0.28
Left anterior descending	4 (29)	29 (45)	15 (75)	15 (65)	1 (17)	1 (17)	
Left circumflex	3 (21)	11 (17)	3 (15)	4 (17)	2 (33)	0 (0)	
Right coronary	7 (50)	24 (38)	2 (10)	4 (17)	3 (50)	5 (83)	
Location of ISR							0.35
Body	12 (86)	42 (66)	10 (50)	15 (65)	3 (50)	4 (67)	
Edge	2 (14)	22 (34)	10 (50)	8 (35)	3 (50)	2 (33)	
Type of ISR							0.41
Focal	10 (71)	42 (66)	17 (85)	14 (61)	5 (83)	5 (83)	
Diffuse	4 (29)	22 (34)	3 (15)	9 (39)	1 (17)	1 (17)	
Stent size (mm)	2.9 ± 0.3	3.0 ± 0.4	2.9 ± 0.4	2.9 ± 0.4	2.8 ± 0.6	3.3 ± 0.3	0.13
Total stent length (mm)	25 ± 6	23 ± 7	22 ± 8	23 ± 6	23 ± 10	21 ± 7	0.64
Stent type							0.001
First generation DES	7 (50)	16 (25)	5 (25)	15 (65)	0 (0)	4 (67)	
Second generation DES	7 (50)	48 (75)	15 (75)	8 (35)	6 (100)	2 (33)	

Data given as mean ± SD or n (%)

DES drug-eluting stent, *ISR* in-stent restenosis

Table 3 Optical coherence tomography analysis

	Type I ($n=14$)	Type II ($n=64$)	Type III ($n=20$)	Type IV ($n=23$)	Type V ($n=6$)	Type VI ($n=6$)	*P* value
Quantitative analysis							
Percent NIH area (%)	78 ± 11	79 ± 11	77 ± 8	80 ± 7	71 ± 24	70 ± 23	0.21
Percent stent expansion (%)	106 ± 27	130 ± 40	124 ± 41	120 ± 32	119 ± 35	90 ± 44	0.07
Qualitative analysis							
Stent fracture (%)	8 (57)	12 (19)	0 (0)	1 (4)	2 (33)	4 (67)	0.22
Plaque rupture (%)	0 (0)	0 (0)	0 (0)	2 (9)	0 (0)	0 (0)	0.08
Microvessels (%)	1 (7)	51 (80)	19 (95)	4 (17)	1 (17)	1 (17)	< 0.001

Data given as mean ± SD or *n* (%)

NIH neointimal hyperplasia

(2) interobserver variability while classifying ISR tissue on OCT by the modified classification was higher than that with the classical classification; (3) all six types of ISR tissues on OCT were clinically significant.

OCT uses near-infrared light and cross-sectional images generated by measuring the echo time delay and intensity of light that is reflected or backscattered from the arterial wall [13]. Because OCT uses near-infrared light, and cross-sectional images are generated by measuring the echo time delay and intensity of light that is reflected or backscattered from the arterial wall, it characterizes tissue morphology by measuring backscattered infrared light. Recently, many ISR tissue types which could not be classified by the classical method have been reported [5–7]. This could have led to the low interobserver variability noted when this method was used in our study. Accordingly, we reviewed 138 OCT images of ISR lesions and classified neointimal tissue characteristics into six patterns. This modified classification enabled us to classify most ISR lesions easily, and certainly with a higher degree of reproducibility. In addition, the clinical significance of these neointimal tissue classifications became clear while using the modified classification.

Type I tissue appeared as homogeneous high-intensity tissue. We have previously reported that homogeneous signal-rich neointima after bare-metal stent and DES implantation was present in the neointimal tissue, composed of smooth muscle cells in a proteoglycan and a collagen-rich matrix, in an ex vivo histological validation study [14, 15]. As OCT measures the intensity of light returning from a tissue, collagen fiber-rich neointima, which has a higher heterogeneity in the optical index of refraction, exhibits stronger optical scattering and, therefore, a stronger OCT signal. In the current analysis, the incidence of stent fracture was predominantly higher in ISR lesions classified as type I. The fractured stent struts may cause continuous mechanical stimulation of the vessel wall, resulting in migration and proliferation of smooth muscle cells within the stent and mobilization of the intimal hyperplasia. Type II tissue appeared as heterogeneous tissue with signal attenuation. The frequency of this type of ISR tissue was the highest in the current analysis. This type of tissue was categorized as layered by the classical classification method and has occasionally been named as peri-strut low-intensity area. Our group has reported that histologically, this type of neointima shows smooth muscle cells with collagen fibers richly distributed on the luminal side and proteoglycan-rich myxomatous matrix in the deeper layer [14, 15]. The proteoglycan-rich myxomatous matrix appears as regions of low backscatter with poor light reflection from tissue; however, the stent struts behind the proteoglycan-rich myxomatous matrix appear as very strong backscattering with shadowing because of strong reflections from the stent struts [15]. A previous study has described that the incidence of fibrin deposition, peri-strut inflammation, and neovascularization was higher in lesions with a layered pattern [3]. These findings may suggest that this type of tissue is a reflection of delayed arterial healing and/or indicates the presence of an organized thrombus. This hypothesis is supported by our findings that the prevalence of microvessels within the low-signal-intensity regions was high in type II tissue. Type III tissue appeared as speckled heterogeneous tissue. This tissue type was categorized as heterogeneous by the classical classification method. Large microvessels within the neointima were identified in 19 lesions (95%), which may represent an organized thrombus. Nagai et al. compared the OCT tissue classification and histology of ISR tissue retrieved by directional coronary atherectomy and reported that heterogeneous pattern indicated neointima comprising organized thrombus and fibrinoids with smooth muscle cells poorly and focally distributed [16]. Similarly, Kim et al. compared the histology and OCT image of ISR tissue and reported that fibrin deposits were more frequently detected in this pattern [3]. The reason for the difference in OCT appearance between types II and III is unclear. We have previously reported on a case showing that neointimal tissue morphology of a DES changed from eccentric speckled heterogeneous tissue to concentric heterogeneous tissue with signal attenuation in 11 months [17]. This finding may suggest that type III tissue may represent the early phase

and type II tissue the late phase in an organized thrombus. Type IV tissue appeared as heterogeneous tissue containing a poorly delineated region with invisible strut. Our group has already reported that this tissue type comprised atheromatous tissue, including large fibroatheroma or a large amount of foam cell accumulation within the neointima on histology [14, 15]. The finding that neointimal rupture was identified only in this tissue type indicates lipidic atherosclerotic neointima in these tissues. These tissues were frequently seen in lesions with first-generation DES, and the duration from stent implantation to ISR was longest in this tissue type. Type V tissue appeared as heterogeneous tissue containing a sharply delineated low-intensity region. A previous ex vivo validation study comparing OCT and histopathological images showed that dense calcified plates appeared as low-signal-intensity areas with sharply delineated borders [18, 19]. In the current analysis, there was a direct connection between neointimal tissue and underlying dense calcified plates. This may indicate that a continuous growth of calcified plates following DES implantation could be one of the mechanisms of ISR after DES. Type VI tissue appeared as bright protruding tissue with an irregular surface. We have reported that this tissue type with similar OCT finding in the native coronary artery was seen as a calcified nodule on histology [15]. The calcified nodule appeared as a low-intensity area with a diffuse border with a high-backscattering protruding mass with an irregular surface on OCT [15]. Although the precise mechanism of calcified nodule development is not clear, it might be associated with the fracture of calcified plates and subsequent fibrin deposition [20]. Therefore, calcified sheets seem to be essential for the pathogenesis of the atherosclerotic calcified nodule. In the current analysis, this tissue type was mostly located at the ostium and middle RCA, which is reported to be a preferred site for calcified nodule development in the native coronary artery [21]. A previous study has revealed that the development of a calcified nodule within the neointima caused ISR after DES implantation [22]. Because this study demonstrated potential to differentiate lipidic atherosclerotic neointima and calcified neointima from other neointimal tissue by the modified classification, this classification may help in guiding treatment strategy and prevention of adverse outcomes for lesions with ISR after DES implantation.

This study had several limitations. First, it involved a retrospective analysis of prospectively collected observational data from a single center. OCT examinations were not performed in all patients who presented with ISR, which could have resulted in a selection bias. Second, OCT examinations were not performed at the time of DES implantation. Therefore, it is unclear whether the underlying plaque morphology behind the stent really affects neointimal tissue characteristics of DES. Third, a relatively small proportion of the study population was involved in the evaluation of the clinical significance of ISR tissue morphology, although over 100 patients who presented with ISR after DES were analyzed. A systemic prospective study is needed to obtain more precise results based on these encouraging preliminary results. Fourth, precisely matched one-to-one OCT finding and histology correlation are lacking. Therefore, its clinical significance was limited because previous study reported that the correlation between OCT image patterns and distinct histological tissue characteristics was weak [23]. Therefore, the clinical implication of the morphological ISR patterns based on OCT findings remains unclear. Fifth, OCT cannot provide definitive differentiation between calcified nodule and red thrombus. Therefore, some of ISR tissue classified into type IV may contain fresh red thrombus even though lesions with stent thrombosis in the 4 weeks prior to the OCT procedure were excluded from the analysis.

Conclusions

OCT can identify six different patterns of ISR tissue after DES implantation. This new modified classification method could be useful in understanding and interpreting the varied images obtained on OCT after DES implantation.

Impact on daily practice

We established a novel optical coherence tomography (OCT) classification of in-stent restenotic tissue after drug-eluting stent (DES) implantation that enabled us to classify most in-stent restenosis lesions easily, and certainly with a higher degree of reproducibility. The clinical significance of these neointimal tissue classifications became clear while using the modified classification. This new modified classification method could be useful in understanding and interpreting the varied images obtained on OCT after DES implantation.

Acknowledgements The authors thank the staffs in the catheterization laboratory at Higashi Takarazuka Satoh Hospital for their excellent assistance during the study.

Funding None.

Compliance with ethical standards

Conflict of interest The authors have no conflict of interest to declare.

References

1. Gonzalo N, Serruys PW, Okamura T, van Beusekom HM, Garcia-Garcia HM, van Soest G, van der Giessen W, Regar E (2009) Optical coherence tomography patterns of stent restenosis. Am Heart J 158:284–293

2. Jinnouchi H, Kuramitsu S, Shinozaki T, Tomoi Y, Hiromasa T, Kobayashi Y, Domei T, Soga Y, Hyodo M, Shirai S, Ando K (2017) Difference of tissue characteristics between early and late restenosis after second-generation drug-eluting stents implantation—an optical coherence tomography study. Circ J 81:450–457
3. Kim JS, Afari ME, Ha J, Tellez A, Milewski K, Conditt G, Cheng Y, Hua Yi G, Kaluza GL, Granada JF (2014) Neointimal patterns obtained by optical coherence tomography correlate with specific histological components and neointimal proliferation in a swine model of restenosis. Eur Heart J Cardiovasc Imaging 15:292–298
4. Xia J, Qu Y, Yin C, Xu D (2017) Optical coherence tomography assessment of glucose fluctuation impact on the neointimal proliferation after stent implantation in a diabetic/hypercholesterolemic swine model. Int Heart J 58:608–614
5. Miura K, Tada T, Habara S, Kuwayama A, Shimada T, Ohya M, Murai R, Amano H, Kubo S, Otsuru S, Tanaka H, Fuku Y, Goto T, Kadota K (2018) Optical coherence tomography predictors for recurrent restenosis after paclitaxel-coated balloon angioplasty for drug-eluting stent restenosis. Circ J 82:2820–2828
6. Murata N, Takayama T, Hiro T, Hirayama A (2018) Balloon pin-hole rupture during percutaneous coronary intervention for recurrent, calcified in-stent restenosis: a case report. Catheter Cardiovasc Interv 91:1287–1290
7. Suna G, Wojakowski W, Lynch M, Barallobre-Barreiro J, Yin X, Mayr U, Baig F, Lu R, Fava M, Hayward R, Molenaar C, White SJ, Roleder T, Milewski KP, Gasior P, Buszman PP, Buszman P, Jahangiri M, Shanahan CM, Hill J, Mayr M (2018) Extracellular matrix proteomics reveals interplay of aggrecan and aggrecanases in vascular remodeling of stented coronary arteries. Circulation 137:166–183
8. Nakazawa G, Otsuka F, Nakano M, Vorpahl M, Yazdani SK, Ladich E, Kolodgie FD, Finn AV, Virmani R (2011) The pathology of neoatherosclerosis in human coronary implants bare-metal and drug-eluting stents. J Am Coll Cardiol 57:1314–1322
9. Finn AV, Otsuka F (2012) Neoatherosclerosis: a culprit in very late stent thrombosis. Circ Cardiovasc Interv 5:6–9
10. Fujii K, Masutani M, Okumura T, Kawasaki D, Akagami T, Ezumi A, Sakoda T, Masuyama T, Ohyanagi M (2008) Frequency and predictor of coronary thin-cap fibroatheroma in patients with acute myocardial infarction and stable angina pectoris a 3-vessel optical coherence tomography study. J Am Coll Cardiol 52:787–788
11. Prati F, Regar E, Mintz GS, Arbustini E, Di Mario C, Jang IK, Akasaka T, Costa M, Guagliumi G, Grube E, Ozaki Y, Pinto F, Serruys PW, EsOR Document (2010) Expert review document on methodology, terminology, and clinical applications of optical coherence tomography: physical principles, methodology of image acquisition, and clinical application for assessment of coronary arteries and atherosclerosis. Eur Heart J 31:401–415
12. Kuramitsu S, Hiromasa T, Enomoto S, Shinozaki T, Iwabuchi M, Mazaki T, Domei T, Yamaji K, Soga Y, Hyodo M, Shirai S, Ando K (2015) Incidence and clinical impact of stent fracture after PROMUS element platinum chromium everolimus-eluting stent implantation. JACC Cardiovasc Interv 8:1180–1188
13. Huang D, Swanson EA, Lin CP, Schuman JS, Stinson WG, Chang W, Hee MR, Flotte T, Gregory K, Puliafito CA (1991) Optical coherence tomography. Science 254:1178–1181
14. Shibuya M, Fujii K, Hao H, Imanaka T, Saita T, Fukunaga M, Miki K, Tamaru H, Nishimura M, Horimatsu T, Naito Y, Ishibashi-Ueda H, Hirota S, Masuyama T (2015) Tissue characterization of in-stent neointima using optical coherence tomography in the late phase after bare-metal stent implantation—an ex vivo validation study. Circ J 79:2224–2230
15. Imanaka T, Fujii K, Hao H, Shibuya M, Saita T, Kawakami R, Fukunaga M, Kawai K, Tamaru H, Miki K, Horimatsu T, Sumiyoshi A, Nishimura M, Hirota S, Masuyama T, Ishihara M (2016) Ex vivo assessment of neointimal characteristics after drug-eluting stent implantation: optical coherence tomography and histopathology validation study. Int J Cardiol 221:1043–1047
16. Nagai H, Ishibashi-Ueda H, Fujii K (2010) Histology of highly echolucent regions in optical coherence tomography images from two patients with sirolimus-eluting stent restenosis. Catheter Cardiovasc Interv 75:961–963
17. Shibuya M, Fujii K, Fukunaga M, Imanaka T, Miki K, Tamaru H, Ohyanagi M, Masuyama T (2015) Natural history of low-intensity neointimal tissue after an everolimus-eluting stent implantation: a serial observation with optical coherence tomography. Heart Vessels 30:136–139
18. Saita T, Fujii K, Hao H, Imanaka T, Shibuya M, Fukunaga M, Miki K, Tamaru H, Horimatsu T, Nishimura M, Sumiyoshi A, Kawakami R, Naito Y, Kajimoto N, Hirota S, Masuyama T (2017) Histopathological validation of optical frequency domain imaging to quantify various types of coronary calcifications. Eur Heart J Cardiovasc Imaging 18:342–349
19. Yabushita H, Bouma BE, Houser SL, Aretz HT, Jang IK, Schlendorf KH, Kauffman CR, Shishkov M, Kang DH, Halpern EF, Tearney GJ (2002) Characterization of human atherosclerosis by optical coherence tomography. Circulation 106:1640–1645
20. Otsuka F, Sakakura K, Yahagi K, Joner M, Virmani R (2014) Has our understanding of calcification in human coronary atherosclerosis progressed? Arterioscler Thromb Vasc Biol 34:724–736
21. Lee T, Mintz GS, Matsumura M, Zhang W, Cao Y, Usui E, Kanaji Y, Murai T, Yonetsu T, Kakuta T, Maehara A (2017) Prevalence, predictors, and clinical presentation of a calcified nodule as assessed by optical coherence tomography. JACC Cardiovasc Imaging 10:883–891
22. Alfonso F, Cuesta J, Bastante T, Aguilera MC, Benedicto A, Rivero F (2016) In-stent restenosis caused by a calcified nodule: a novel pattern of neoatherosclerosis. Can J Cardiol 32:830.e1–3
23. Lutter C, Mori H, Yahagi K, Ladich E, Joner M, Kutys R, Fowler D, Romero M, Narula J, Virmani R, Finn AV (2016) Histopathological differential diagnosis of optical coherence tomographic image interpretation after stenting. JACC Cardiovasc Interv 9:2511–2523